Solid state to solution: crystal structure and molecular dynamics simulations of a polyammonium nitrate host

Joanna Wiórkiewicz-Kuczera,[a] Krzysztof Kuczera,[a] Carla Bazzicalupi,[b] Andrea Bencini,[b] Barbara Valtancoli,[b] Antonio Bianchi,[b]* and Kristin Bowman-James[a]*

[a] *Department of Chemistry, University of Kansas, Lawrence, Kansas 66045, USA.*
[b] *Department of Chemistry, University of Florence, 50144 Florence, Italy*

Received (in New Haven, USA) 21st January 1999, revised manuscript received 6th August 1999, Accepted 6th August 1999

The crystal structure of a hexaprotonated octaaza macrocycle, 1,4,7,10,13,16,19,21-octaazacyclotetracosane, has been obtained as the nitrate complex, $H_8\mathbf{1}\cdot 8NO_3$. The complex crystallizes in the monoclinic space group $P2_1/c$ with unit cell parameters $a = 14.43(2)$, $b = 8.36(1)$, $c = 15.9(1)$ Å, $\beta = 110.8(2)^\circ$ and $U = 1793(12)$ Å^3. The macrocycle crystallizes in a relatively flat elliptical conformation with dimensions of 11.9 and 7.2 Å, and a depth of 1.8 Å. The crystallographic coordinates formed the basis for molecular dynamics simulations over a 400 ps timeframe using the all-atom CHARMM version 25 package. The major change in the conformational structure of the macrocycle during the simulations was the shifting of all NCCN dihedral angles to a *trans* conformation. Also, each conformational transition in CNCC and CCNC angles flanking a central CC bond was found to be correlated. The macrocycle remained relatively flat throughout the simulation, resulting in essentially complete hydration within the first 100 ps of the simulation. Extensive water relay networks could be identified throughout the simulation, which are attributed to maintaining and stabilizing anion/cation interactions in solution.

Developments in the field of anion recognition have relied heavily on the wide variety of shapes and sizes provided by polyammonium macrocyclic receptors. By virtue of their hydrogen bonding and protonation capabilities even at neutral pHs, these molecules are ideally suited as receptors for anions. They have, in fact, proven capabilities in binding ranging from simple monatomic halides to polyatomic oxo anions such as nitrates and phosphates, and even to complex organic systems including nucleotides and polycarboxylic acids.[1] Designing systems that selectively recognize a given anion over others is not simple, however. For example, electrode selectivity for anions usually follows the Hofmeister series, a pattern based on lipophilicity.[2]

Our interest in designing selective receptors for various oxo anions of environmental relevance has led us to an examination of systems capable of forming complexes with nitrate.[3,4] Nitrate is present in massive quantities in the radioactive waste tanks at Hanford,[5] and also is found in groundwaters, where it may pose significant health risks.[6] As part of our investigation, we have sought to obtain solid state structural data for a variety of macrocyclic complexes containing nitrate. It is true, however, that while crystallographic information can indicate certain binding preferences, interactions in solution can be vastly different. This is especially the case in aqueous systems, where hydration effects often overpower the selective abilities of ion receptors.

Molecular dynamics (MD) simulations of complex chemical systems can provide a powerful tool in examining the solution properties of a variety of chemical species, resulting in a greater in-depth understanding of the physico-chemical properties, structure, dynamics and function of molecules in solution.[7] The power of MD simulations lies in the detailed information that can be obtained by probing motions of individual atoms on a subpicosecond time scale. MD simulations have been successfully applied to a number of macrocyclic systems in recent years, yielding insight into the structure, preorganization and mechanisms of complexation of a variety of host–guest systems.[8] With respect to anions, MD studies involving macrocyclic receptors have been limited, however, mostly involving halide guests, including the spherical "soccer ball" ligand[9,10] and simple amine-based monocycles.[11,12]

In our continued interest in nitrate, as well as in our continuing efforts to bridge the gap between the solid state and solution chemistry, we have used the crystallographic data obtained for a 24-membered octaprotonated octaaza macrocycle, 1,4,7,10,13,16,19,21-octaazacyclotetracosane, $\{H_8([24]aneN_8)\}\cdot(8NO_3)$, $H_8\mathbf{1}\cdot 8NO_3$, as a basis for MD simulations. A related study by several of us focussed on the solution behavior of two polyammonium macrocycles differing in ring size: 1,4,10,13-tetraaza-7,16-dioxacyclooctadecane, $[18]aneN_4O_2$ (**2**), and 1,4,7,16,19,21-hexaaza-10,13-dioxacyclotetracosane, $[24]aneN_6O_2$ (**3**).[3] In that earlier report the influence of solvation and ring size on macrocyclic conformation was probed. Of particular interest here is that **1** is a direct corollary of **3** with respect to ring size and make-up, but with amines replacing the two oxygen atoms in the ring. In contrast, however, **1** exhibits a considerably higher degree of protonation ($8H^+$ compared to $4H^+$) as well as a totally different conformation in the crystal structure compared to **3**.

Experimental

Synthesis of $\{H_8([24]aneN_8)\}\cdot(8NO_3)$, $H_8\mathbf{1}\cdot 8NO_3$

The macrocycle **1** was synthesized according to previously reported methods.[13] Crystals of $H_8\mathbf{1}\cdot 8NO_3$ suitable for X-ray analysis were obtained by slow evaporation at room temperature of a solution of the macrocycle in 0.1 mol dm^{-3} aqueous HNO_3.

Crystal structure resolution and refinement

Crystallographic data for $H_8\mathbf{1}\cdot 8NO_3$ are summarized in Table 1. A colorless prismatic crystal of the compound (approximate dimensions 0.30 mm × 0.07 mm × 0.05 mm) was mounted on an Enraf-Nonius CAD4 X-ray diffractometer with equatorial geometry. Data were collected at room temperature with graphite-monochromated Mo-Kα radiation ($\lambda = 0.71069$ Å). Cell parameters were determined by a least-

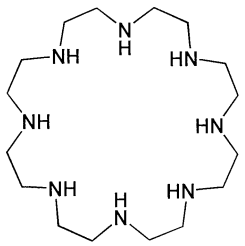

1

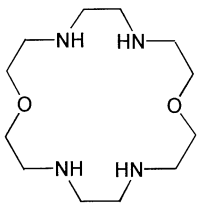

2

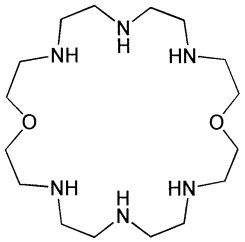

3

squares refinement of diffractometer setting angles for 25 carefully centered reflections. The intensities of two standard reflections were monitored during data collection and showed no loss of intensity. Intensity data were corrected for Lorentz and polarization effects, and an absorption correction was applied using the method of Walker and Stuart.[14]

The structure was solved by direct methods using the SIR-92 program.[15] Anisotropic thermal parameters were used for all non-hydrogen atoms. Hydrogen atoms bound to ligand carbon atoms were included as calculated positions, and their coordinates were refined in conjunction with the linked atoms, giving an overall isotropic temperature factor refined to a final value of 0.031 Å^2. The eight hydrogen atoms bound to ligand nitrogen atoms were introduced in calculated positions, with an overall isotropic temperature factor refined to a final value of 0.050 Å^2.

Refinements (215 parameters) were performed using full-matrix least-squares methods with the SHELXL-93[16] program, which uses the analytical approximation for the atomic scattering factors and anomalous dispersion corrections[17] for all the atoms. Selected bond distances and angles are provided in Table 2.

CCDC reference number 440/137. See http://www.rsc.org/suppdata/nj/1999/1007/ for crystallographic files in .cif format.

Molecular dynamics simulations

MD simulations were performed for $H_8\mathbf{1}\cdot 8NO_3$ using the CHARMM version 25 package with the all-atom topology and parameters.[18,19] Additional parameters for secondary ammonium cation nitrogens were developed earlier in our group.[3] The initial molecular coordinates were obtained from the crystal structure data. Simulations were carried out for a system containing one H_8[24]aneN$_8{}^{8+}$ macrocycle, eight nitrates and 1152 waters, with 3560 atoms altogether. The van der Waals interactions were truncated by applying an energy switching function between 10 and 12 Å in order to eliminate discontinuities due to the cutoff.[19] Two schemes were used for calculating electrostatic interactions: cutoff and Ewald. In the cutoff scheme the electrostatic interactions were truncated at 12 Å through a shift function.[19] In the Ewald scheme, the Particle-Mesh Ewald method as implemented in CHARMM version 25 was used to evaluate electrostatics. In this method truncation is avoided by considering contributions from an infinite array of periodic images of the primary cell. Molecular dynamics simulations were carried out under constant temperature and pressure conditions of 300 K and 1 atm ($\approx$101 kPa) with a time step of 2 fs, SHAKE constraints applied to bonds involving hydrogen atoms,[20] and cubic periodic boundary conditions. The cutoff and Ewald treatments of electrostatics were then used in two separate simulations. In each case initial preparation involved 10 ps of solvent equilibration with the macrocycle fixed in the crystal geometry, 10 ps of full system equilibration, followed by 400 ps of trajectory generation. The cube edges were 32.55 $\pm$ 0.09 Å in the cutoff and 32.71 $\pm$ 0.09 Å in the Ewald simulations.

Table 1 Crystal data and structure refinement for $\{H_8$([24]aneN$_8)\}\cdot(8NO_3)$

Empirical formula	$C_{16}H_{48}N_{16}O_{24}$
Formula weight	848.70
Crystal system	Monoclinic
Space group	$P2_1/c$
a/Å	14.43(2)
b/Å	8.360(10)
c/Å	15.90(10)
β/°	110.8(2)
U/Å^3	1793(12)
Z	2
T/K	293
μ/cm^{-1}	1.46
Total reflections	1727
Reflections with $I > 2\sigma(I)$	1470
R^a	0.0402
R_w^2 ^{b}	0.1076

^{a} $R = \|F_o\| - |F_c\|/|F_o|$. ^{b} $R_w^2 = [w(F_o^2 - F_c^2)^2/wF_o^4]^{1/2}$, $w = 1/[\sigma^2(F_o^2) + (0.0649P)^2 + 1.23P]^{1/2}$, $P = F_o^2/3 + 2F_c^2/3$.

Table 2 Selected bond lengths (Å) and angles (deg) for $\{H_8$([24]aneN$_8)\}\cdot(8NO_3)$

Macrocycle		Nitrates	
N1–C8	1.486(5)	N5–O51	1.268(7)
N1–C1	1.499(5)	N5–O52	1.228(4)
C1–C2	1.500(4)	N5–O53	1.267(7)
C2–N2	1.504(8)	N6–O61	1.244(6)
N2–C3	1.492(4)	N6–O62	1.231(4)
C3–C4	1.522(8)	N6–O63	1.266(7)
C4–N3	1.501(6)	N7–O71	1.262(7)
N4–C7	1.482(6)	N7–O72	1.230(4)
C7–C8	1.513(5)	N7–O73	1.241(5)
C8–N1	1.486(5)	N8–O81	1.270(6)
		N8–O82	1.249(6)
		N8–O83	1.232(4)
Macrocycle		**Nitrates**	
C8–N1–C1	113.3(4)	O51–N5–O52	120.2(3)
N1–C1–C2	113.8(2)	O51–N5–O53	119.4(4)
C1–C2–N2	113.2(3)	O52–N5–O53	120.5(3)
C3–N2–C2	111.7(3)	O61–N6–O62	121.8(4)
N2–C3–C4	113.0(3)	O61–N6–O63	120.1(4)
N3–C4–C3	115.0(3)	O62–N6–O63	118.1(4)
C5–N3–C4	114.8(3)	O71–N7–O72	120.7(3)
N3–C5–C6	109.6(3)	O71–N7–O73	119.0(4)
N4–C6–C5	110.2(3)	O72–N7–O73	120.4(3)
C7–N4–C6	115.2(3)	O81–N8–O82	118.9(4)
N4–C7–C8	108.6(4)	O81–N8–O83	119.6(3)
N1–C8–C7	110.8(3)	O82–N8–O83	121.5(3)

Results and discussion

Crystal structure of $H_8\mathbf{1}\cdot 8NO_3$

The molecular structure consists of an octaprotonated cation, H_8[24]aneN$_8{}^{8+}$, $H_8\mathbf{1}^{8+}$, and eight nitrate counterions (ORTEP diagram,[21] Fig. 1). Each macrocyclic cation lies around a crystallographic inversion center, approximately flattened on a plane [deviation from the mean plane described by the nitrogen atoms lying in the range 0.135(3)–0.718(3) Å for N2 and N4, respectively]. The geometry may be viewed as an ellipse with x and y axes equal to 11.9 Å and 7.2 Å, respectively, and the height z equal to 1.8 Å. This flattened structure differs considerably from that observed for the nitrate complex of **3**, in which the macrocycle has a distinct boat shape in the solid state with a deep cavity incorporating one nitrate ion.[3]

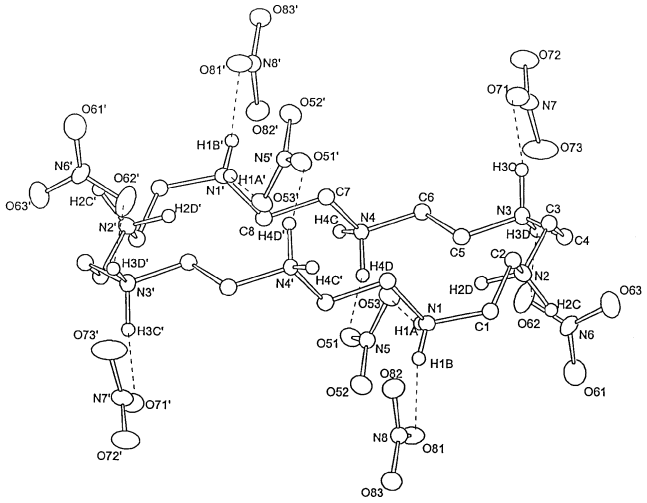

Fig. 1 ORTEP view of $\{H_8([24]aneN_8)\}\cdot(8NO_3)$ including hydrogen bonding contacts between the nitrates and macrocycle.

The structural difference is interesting since the two macrocycles differ only in the presence of the two oxygen atoms instead of amines in **3** and in the degree of protonation. (As noted earlier, in the nitrate structure of **3** the macrocycle crystallized in the tetraprotonated form.) Whether the oxygen atoms and/or the degree of protonation play a major role in the conformation are distinct possibilities, and these questions are currently under investigation.

In the solid state $H_8\mathbf{1}^{8+}$ adopts a conformation in which the NCCN, CCNC, and CNCC dihedral angles are found in the *trans* (*t*) (*ca.* 180°), *gauche*$^-$ (g^-) (from −109° to −58°), and *gauche*$^+$ (g^+) (from 58° to 109°) regions. Four NCCN dihedral angles were found in the *t* conformation (N3–C5–C6–N4, N4–C7–C8–N5 and their symmetry-related counterparts), two in the g^- conformation (N1–C1–C2–N2 and its counterpart), and two in the g^+ conformation (N2–C3–C4–N3 and its counterpart) (Table 3). The crystallographic values for four CCNC angles belong to the *t* region (C1–C2–N2–C3, C7–C8–N1′–C1′ and their symmetry relatives), with the remaining four angles equally split between the g^- and g^+ domains (two at *ca.* ±60° and two close to ±90°). The crystallographic values of six CNCC angles are within the *t* region, and the remaining two angles are found in *g* domains (C8–N1′–C1′–C2′ and its symmetry-related analog) (*ca.* ±75°).

Table 3 Dihedral angles from crystallographic data for $\{H_8([24]aneN_8)\}\cdot(8NO_3)$

N1–C1–C2–N2	−75.8(4)	N3–C5–C6–N4	−179.1(3)
C1–C2–N2–C3	−175.6(3)	C5–C6–N4–C7	85.4(4)
C2–N2–C3–C4	174.5(3)	C6–N4–C7–C8	172.9(3)
N2–C3–C4–N3	99.4(4)	N4–C7–C8–N1′	−165.8(3)
C3–C4–N3–C5	−55.6(4)	C7–C8–N1′–C1′	168.8(3)
C4–N3–C5–C6	178.8(3)	C8–N1′–C1′–C2′	73.3(4)

Each nitrogen atom is protonated, and the electrostatic repulsion forces all of these acidic protons to point outside the macrocyclic cavity. The conformation assumed by the protonated ligand thus gives rise to considerable strain within the molecule. In particular, the C–N–C bond angles show significantly high values [113.3(3)°, 111.6(3)°, 114.8(3)°, 115.2(3)° for N1, N2, N3 and N4, respectively]. The high angular values found for N1, N3 and N4 could probably be explained by the fact that both protons bound to these nitrogens are involved in strong hydrogen bond interactions with the nitrate ions. In fact, H1A and H1B interact with O53 and O81, respectively [N1···O53 = 2.88(1) Å and N1···O81 = 2.744(5) Å]. H3C and H3D interact with O71 and O62, respectively [N3···O62 = 2.89(2) Å and N3···O71 = 2.899(5) Å]. O51 gives rise to a bridging interaction with H4D and H4D″ belonging to a symmetry-related molecule [N4···O51 = 2.828(5) Å and N4″···O51 = 2.84(1) Å; symmetry operation for N4″ = x, $-y-0.5$, $z+0.5$]. The remaining nitrogen atom, N2, is involved only in a single hydrogen bond contact with a symmetry-related nitrate [N2···O63″ = 2.777(5) Å; symmetry operation: $-x-1$, y, $-z$].

It is worth noting that while six of the associated nitrates are held *via* a single hydrogen bond linkage to the macrocycle, oxygen atoms belonging to N5 and N5′ form a hydrogen bond bridge across the macrocycle. These two nitrates are related by the crystallographic inversion center and lie on opposite sides of the nitrogen-containing plane. They thus are partially included into the macrocyclic framework. This dual linkage tends to pull the two sides of the macrocycle together as can be seen more clearly in Fig. 2.

Hydrogen bonding effects also play a major role in the macrocyclic packing within the crystal structure, with symmetry-related macrocycles being bridged by O51 and by O63. This intermolecular hydrogen bond network gives rise to a remarkably compressed crystal packing (Fig. 3). This "denseness" is also reflected in the value of the calculated

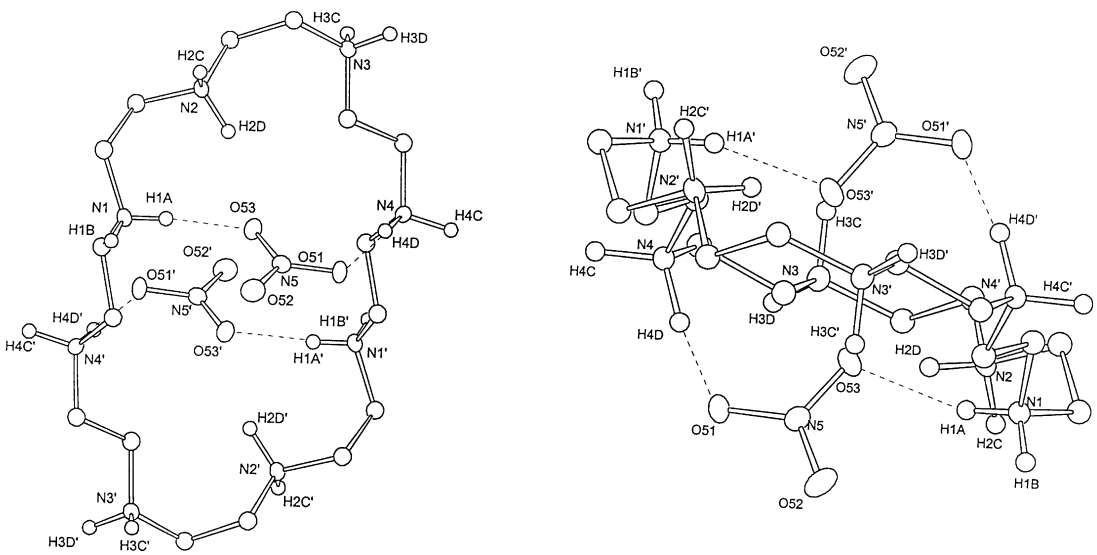

Fig. 2 ORTEP view of $H_8([24]aneN_8)$ with $N5O_3^-$ and $N5'O_3^-$ showing hydrogen bonding across the macrocycle from overhead and side views.

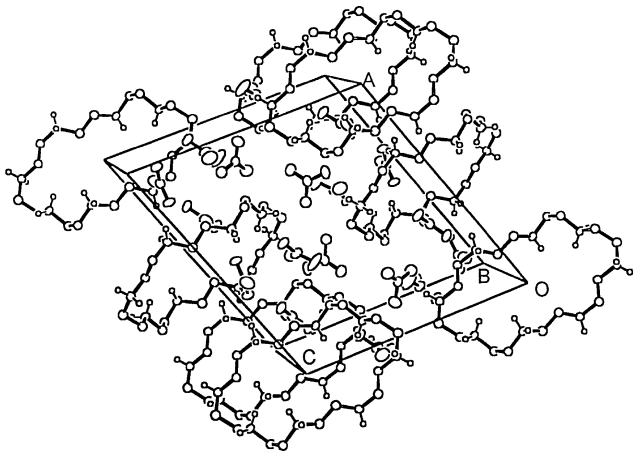

Fig. 3 Packing diagram of the crystal structure of $\{H_8([24]aneN_8)\}\cdot(8NO_3)$.

density of the crystal, 1.6 g cm^{-3}, which is rather high for an organic compound.

Molecular dynamics simulations

Conformation of the macrocycle. The macrocycle lost its crystallographic symmetry during the simulations. However, the overall shape of **1** did not change significantly, as may be seen in Fig. 4, which shows the molecular dimensions during the simulations. The macrocycle shapes found in the Ewald and cutoff simulations were essentially the same and quite similar to that in the crystal structure. This finding is in contrast to the previously reported simulations performed on the boat-shaped macrocycle **3**, which flattened considerably over the course of 400 ps to become essentially the same overall shape as **1**.[3]

During both the cutoff and Ewald simulations, all eight NCCN angles adopted a *t* conformation (Fig. 5). The repulsive electrostatic interaction between the positively charged ammonium groups tends to make the *t* conformer the most energetically favorable in aqueous solution. In the crystal structure, four of the CCNC angles were *t* and two each were in the g^- and g^+ regions, while of the CNCC angles, six were in the *t* region and two were in the *g* domains. The simulation results showed some deviations from this pattern. In the cutoff

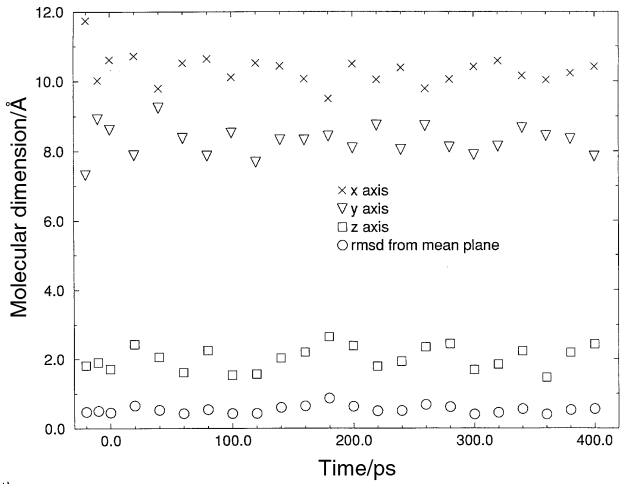

Fig. 4 Variation of macrocycle shape and size during the simulation. Plots show dimensions (Å) along the three principal axes of the moment of inertia (*x*, *y*, *z*) and the non-hydrogen atom root-mean-square deviation from the mean molecular plane. Values calculated for structures were sampled from the molecular dynamics trajectory every 20 ps (20–400 ps), as well as the crystal structure (−20 ps), and structures after heating (−10 ps) and equilibration (0 ps). The results shown are for the cutoff simulation; the Ewald simulation results were practically identical and are not shown for clarity.

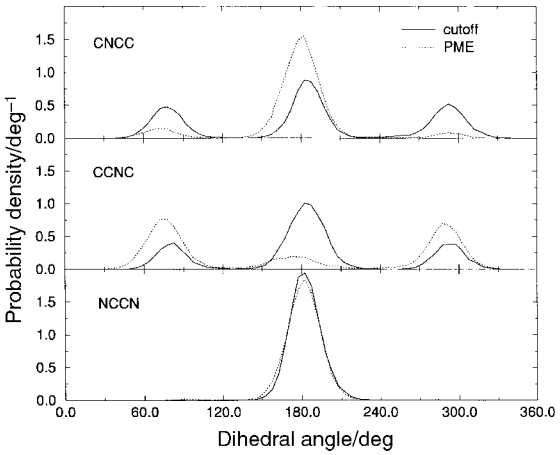

Fig. 5 Probability distributions of the macrocycle dihedral angles sampled during the molecular dynamics simulation. Solid line: cutoff simulation; dotted line: Ewald simulation using the Particle-Mesh Ewald (PME) method.

simulation, the general pattern of the CCNC conformations was the same as in the crystal, while of the CNCC angles, four were in *t* and four were in *g* regions (Fig. 5). As a result, typical non-hydrogen atom rms deviations from the crystal structure were 0.9 Å. In the Ewald simulation, two of the CCNC dihedrals were *t* and six were in the *g* regions; six of the CNCC angles were in *t*, with two in the *g* domains. This pattern led to a somewhat smaller rms deviation from the crystal structure: typically 0.6 Å. Interestingly, the conformational conversions in CNCC and CCNC dihedrals were highly correlated—a *t* to *g* or *g* to *t* change in C($i-2$)–N($i-1$)–C(i)–C($i+1$) was usually accompanied by a corresponding *g* to *t* or *t* to *g* transition of C(i)–C($i+1$)–N($i+2$)–C($i+3$). Such correlated transitions tended to conserve the macrocycle shape.

Nitrate motions. The time evolution of the distances between the nitrates and the macrocycle center is presented in Fig. 6(*A*)–(*H*). The corresponding distance probability distributions are presented in Fig. 7(*A*)–(*H*). The simulation results show several interesting effects. First, one nitrate always remains bound inside the central macrocycle cavity. In the cutoff simulation this centrally bound ion is nitrate $N5O_3^-$ during the first 30 ps, and nitrate $N8'O_3^-$ in the remainder of the trajectory. In the Ewald simulation, the same nitrates are involved, but the exchange occurs much later, at *ca.* 220 ps. A second group of nitrate ions is found residing mostly within 15 Å of the macrocycle center. These are nitrates $N7O_3^-$ and $N6O_3^-$ in the cutoff simulation, and $N8O_3^-$ and $N8'O_3^-$ (prior to its binding to the central cavity) in the Ewald trajectory. The remaining nitrate ions explore a wide range of distances from the macrocycle center, up to the largest possible in the simulation cell. This largest distance is equal to half the cube diagonal, or about 26 Å in both simulations. In our calculations we have centered the periodic images on the macrocycle center, so that the distances reported are the closest possible under the imposed periodic boundary conditions.

The bound nitrate remains within 3 Å of the macrocycle center in both of our simulations, executing tumbling motions. Typically, this anion is involved in two hydrogen bonds with the ammonium groups of **1**. This is analogous to the situation with **3** reported previously, where a central nitrate remained essentially within the cavity throughout the simulation.[3] The difference is that in our current simulations we see an exchange of the bound nitrate within the 400 ps trajectories. Since only one exchange event was observed per trajectory, we cannot reliably determine the time scale of this process.

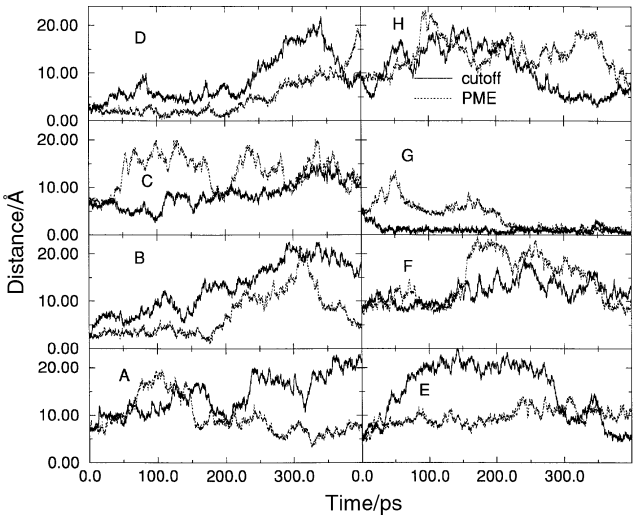

Fig. 6 Time evolution of the distance between individual nitrate nitrogens and the macrocycle center in the molecular dynamics simulations. The macrocycle center is defined as the center of mass of the eight NH_2^+ nitrogens. Solid line: cutoff simulation; dotted line: Ewald simulation. (*A*) Nitrate N7′; (*B*) nitrate N5′; (*C*) nitrate N7; (*D*) nitrate N5; (*E*) nitrate N8; (*F*) nitrate N6; (*G*) nitrate N8′; (*H*) nitrate N6′.

The nitrates that remained at intermediate distances of 5–15 Å from the macrocycle were involved in direct (single and bifurcated) hydrogen bonds to the macrocycle, as well as in water-mediated interactions. These latter interactions tend to be very important for the stabilization of the complex, and will be discussed in greater detail in the section on hydration below.

Due to the constraints of crystal packing in the starting structure, all nitrates were initially within 8 Å of the macrocycle center. By the end of the 400 ps trajectories, the anions were redistributed much more evenly. A summary of this distribution is given in the bottom half of Fig. 8, which shows the average number of nitrates $N(r)$ residing within a distance r of the macrocycle center. For the cutoff simulation the average from the whole trajectory is shown (solid line). In this case the nitrate distribution quickly reached equilibrium, and the $N(r)$ distributions from the first and last 100 ps of the trajectory were essentially identical. For the Ewald simulation the results from the last 100 ps are shown (dotted line). In this case the $N(r)$ distribution showed significant variation between the start and end of the trajectory. It thus appears that the relaxation of the nitrate cloud around **1** is slower in the Ewald simulation, and takes place over at least 200 ps. The distributions in Fig. 8 clearly show the presence of one nitrate inside the macrocycle cavity. Three additional ntirates reside within 5–15 Å of the macrocycle center, while four are on average more than 15 Å distant.

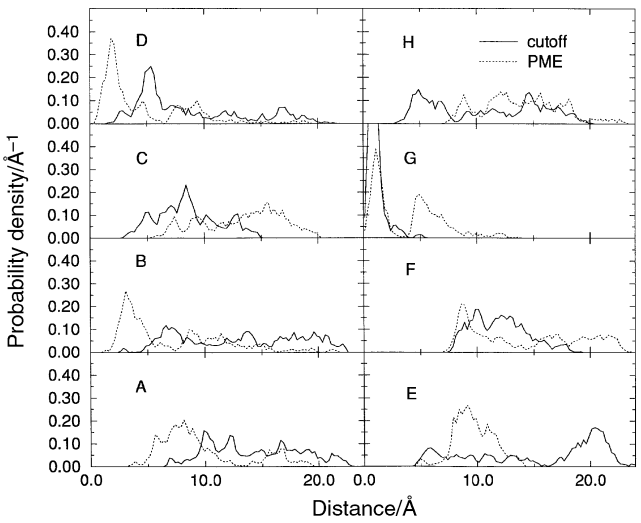

Fig. 7 Probability distributions of the distance between individual nitrate nitrogens and the macrocycle center sampled in the molecular dynamics trajectories. Solid line: cutoff simulation; dotted line: Ewald simulation. (*A*)–(*H*) same as in Fig. 6.

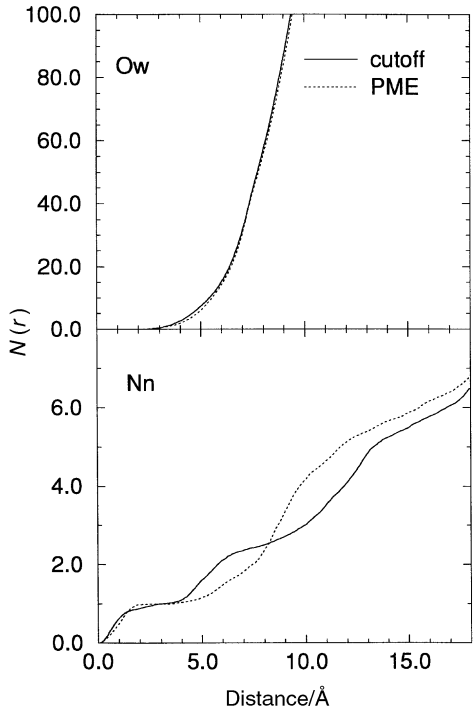

Fig. 8 Distribution of water molecules (Ow) and nitrates (Nn) around the macrocycle center during the molecular dynamics simulations. The vertical axis gives $N(r)$, the average number of species present within a distance r of the macrocycle center. Solid line: cutoff simulation; dotted line: Ewald simulation. For water, averages over the full 400 ps trajectories are given. For nitrates, the cutoff result (solid line) corresponds to the full 400 ps average, while the Ewald data are for the final 100 ps of the trajectory.

The $N(r)$ distributions calculated from the cutoff and Ewald trajectories differ in details. The largest deviations appear in the 8–12 Å range of distances—close to where the results of the truncation of electrostatic interactions might be expected to be most severe. However, the general picture of one nitrate bound inside the macrocycle and the remaining seven redistributed throughout the simulation cell is the same in both the cutoff and Ewald trajectories.

Hydration of the macrocycle and nitrates. It is clear that hydration effects are extremely important in solution chemistry. For example, in earlier studies the presence of water was found to have a major influence on NCCN conformations in ethylenediamine.[11] While the *t* conformation was found to be a global minimum, the presence of water could allow for the existence of the *g* form as a local minimum. Likewise, in this study, as in our previous investigation,[3] water and the resulting hydrogen-bonding microstructures play major roles in complex and conformation stabilization.

The number of water molecules within 7 Å of the macrocycle center of mass was approximately 30 in both simulations Fig. 8, top). This number did not change significantly during the course of the simulations, and was the same in the cutoff and Ewald trajectories. In both cases, the solvent reorganization appears to be complete within the first 100 ps. These results suggest that the macrocycle was accessible to water from the beginning of the simulations due to its relatively flat conformation. Subsequent conformational changes in the macrocycle did not affect its hydration, as it retained its oval shape and remained fairly flat. The rapid hydration observed for $H_8\mathbf{1}^{8+}$ is in contrast to the slower process found for the

nitrate complex of **3**.[3] In the latter case, the hydration was complete only after 200 ps of simulation and involved considerable structural changes.

As was found for the macrocycle, the nitrates were also accessible to water molecules from the beginning of the simulation. The number of water molecules surrounding individual nitrates correlated with their distance from the macrocycle, and, as anticipated, increased with increasing distance from the macrocycle. For example, for $N5'O_3^-$ the average number of waters around it within a 6 Å sphere was 22–23 when the nitrate was within 3–8 Å of the nearest macrocycle center at the start of the simulations. This number increased to 26 when the nitrate moved more than 10 Å away from the macrocycle. Similar hydration changes could be seen for the other nitrates.

Closely correlated with solvation effects were the water-mediated interactions between the macrocycle and the three nitrates found at distances ranging from 3–12 Å from the nearest amino group. These interactions undoubtedly play an important role in the stabilization of this complex and other such complexes. During the outbound excursions (5–12 Å) of these nitrates, water bridges ranging from one to five water molecules were observed, spanning the distance between the macrocycle ammonium hydrogens and the nitrate oxygens. Examples of these networks can be seen in Fig. 9, which shows the water relays from the macrocycle to $N8O_3^-$ at selected times during the course of the simulation. At 20 ps, there was a bridge from N1 through a single water molecule to N8 at an N···N distance of 5.2 Å [Fig. 9(*A*)]. At 60 ps two relays served to tie N8 to N2′ at a distance of 7.3 Å [Fig. 9(*B*)]. A bridge of five water molecules connected N3′ to N8 at 80 ps at a distant 11.4 Å [Fig. 9(*C*) and 9(*D*), side and overhead views, respectively]. Another instance of two water relays, this time connecting N8 to N3′, was found at 100 ps. with N···N = 5.2 Å [Fig. 9(*E*)]. At 140 ps a single bridge connected N8 to the macrocycle, this time again to N1 at a distance of 5.4 Å [Fig. 9(*F*)]. In this latter case, the nitrate also resided close to the internal nitrate, $N5O_3^-$, still sitting in the center of the macrocycle, with N8···N5 = 4.8 Å [Fig. 9(*G*)]. Thus, as indicated in previous studies,[3,11] the solvent plays a crucial role in the organization of the anion–macrocycle complex, and analysis of the water structure provides considerable insight into the ability of the receptor to bind anions.

Conclusions

The macrocycle, which crystallized in the octaprotonated form, was found to have a rather flat conformation in the solid state. Two of the eight nitrates, $N5O_3^-$ and $N5'O_3^-$, were more closely associated with the macrocycle compared to the others, and formed a hydrogen-bonded bridge across the macrocycle. As a result of these interactions the two "sides" of the macrocycle involved in the bridge are pulled closer to each other, resulting in the formation of an ellipse-like structure. These results contrast significantly to those obtained for the nitrate complex of $H_4\mathbf{3}^{4+}$.[3]

The major change in the conformational structure of the macrocycle during the simulations was the shifting of all NCCN dihedral angles to a *trans* conformation, in which electrostatic repulsion between charged amino groups was mini-

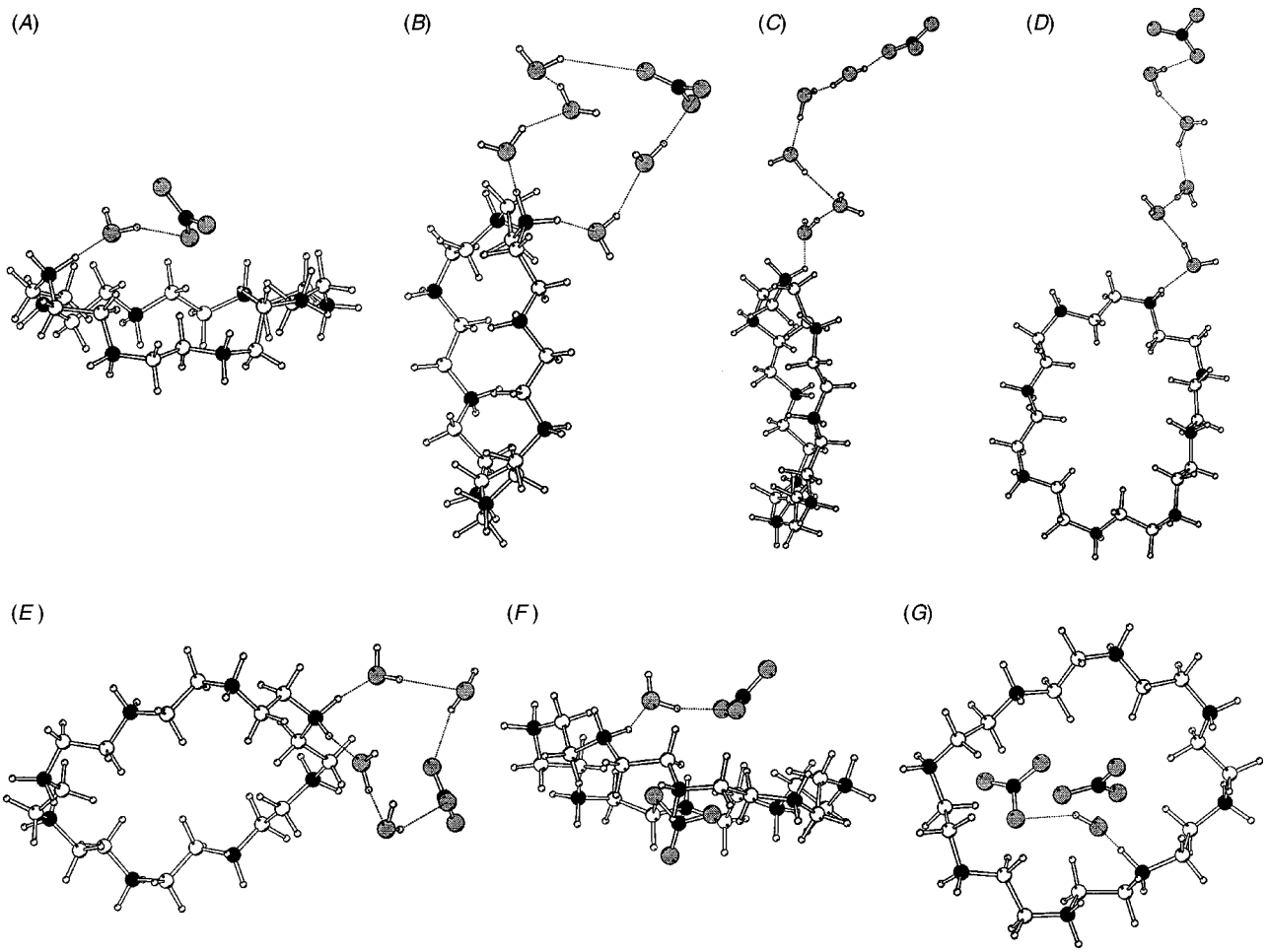

Fig. 9 Sample structures from molecular dynamics trajectory showing several macrocycle–water–nitrate hydrogen bond networks involving nitrate $N8O_3^-$. (*A*) t = 20 ps, interaction involves macrocycle N1; (*B*) t = 60 ps, interaction involves macrocycle N16; (*C*) t = 80 ps, interaction involves macrocycle N19, side view; (*D*) overhead view of (*C*); (*E*) t = 100 ps, interaction involves macrocycle N19; (*F*) t = 140 ps, interaction involves macrocycle N1 and also shows nitrate $N5'O_3^-$ sitting in the macrocycle; (*G*) overhead view of (*F*).

mized. Throughout the simulation all conformational transitions in CNCC and CCNC angles flanking a central CC bond were found to be correlated, so that the observed conformational changes did not affect the overall shape of the macrocycle. The macrocycle also remained relatively flat throughout the simulation, making it immediately accessible to water. This resulted in a rapid hydration pattern, which developed within the first 100 ps of the simulation.

In the molecular dynamics simulations we found that one nitrate continues to occupy the central cavity of the macrocycle, while the remaining anions tend to explore distances from 5 to 26 Å from the macrocycle center, the latter being the largest possible separation in our simulation cell. This picture of nitrate redistribution in solution relative to the crystal is an example of the usefulness of computational methods, which can provide information complementary to experimental studies.

Most importantly, however, hydration effects were found to have a major influence on the interactions between the macrocycle and the nitrates. In this regard, extensive water relay networks could be identified throughout the simulation, which tended to maintain and stabilize interactions between the cationic macrocycle and negatively charged nitrates. These types of interactions undoubtedly play major roles in solution chemistry, not only for relatively simple systems such as this, but also for more complex host–guest/receptor–substrate systems as found throughout nature.

Acknowledgements

This work was supported by the Department of Energy Grant Number DE-FG07-96ER62307 and the NSF EPSCoR initiative.

References

1 (*a*) *Supramolecular Chemistry of Anions*, eds. A. Bianchi, K. Bowman-James and E. García-España, Wiley-VCH, New York, 1997. (*b*) P. D. Beer, J. W. Wheeler and C. Moore, in *Supramolecular Chemistry*, eds. V. Balzani and L. De Cola, Kluwer Academic Publishers, Dordrecht, 1992, pp. 105–118. (*c*) H. E. Katz, in *Inclusion Compounds*, eds. J. L. Atwood, J. E. D. Davies and D. D. MacNichol, Oxford University Press, Oxford, 1991, pp. 391–405. (*d*) C. Seel, A. Galan and J. deMendoza, *Top. Curr. Chem.*, 1995, **175**, 101.
2 F. Hofmeister, *Arch. Exp. Pathol. Pharmakol.*, 1888, 247.
3 G. Papoyan, K. Gu, J. Wiórkiewicz-Kuczera, K. Kuczera and K. Bowman-James, *J. Am. Chem. Soc.*, 1996, **118**, 1354.
4 S. Mason, T. Clifford, L. Seib, K. Kuczera and K. Bowman-James, *J. Am. Chem. Soc.*, 1998, **120**, 8899.
5 D. L. Illman, *Chem. Eng. News*, 1993, June 21.
6 D. C. Bouchard, M. K. Williams and R. Y. Surampalli, *J. Am. Water Works Assoc.*, 1992, **84**, 85.
7 (*a*) C. L. Brooks, III, M. Karplus and B. M. Petitt, *Proteins: A Theoretical Perspective of Dynamics, Structure, and Thermodynamics*, John Wiley and Sons, New York, 1988. (*b*) W. F. van Gunsteren and H. J. C. Berendsen, *Angew. Chem., Int. Ed. Engl.*, 1990, **29**, 992.
8 (*a*) G. Rangina, M. S. Romano, J.-M. Lehn and G. Wipff, *J. Am. Chem. Soc.*, 1985, **107**, 7873. (*b*) T. P. Straatsma and J. A. McCammon, *J. Chem. Phys.*, 1989, **91**, 3631. (*c*) P. Cieplak and P. Kollman, *J. Chem. Phys.*, 1990, **92**, 6761. (*d*) S. D. Liem and P. A. Kollman, *J. Chem. Phys.*, 1995, **99**, 55. (*e*) Y. L. Ha and A. K. Chakraborty, *J. Chem. Phys.*, 1991, **95**, 10781. (*f*) L. Troxler and G. Wipff, *J. Am. Chem. Soc.*, 1994, **116**, 1468. (*g*) G. A. Forsyth and J. C. Lockhart, *J. Chem. Soc., Dalton Trans.*, 1994, 697. (*h*) C. I. Bayly and P. A. Kollman, *J. Am. Chem. Soc.*, 1994, **116**, 697. (*i*) B. E. Thomas, IV and P. A. Kollman, *J. Am. Chem. Soc.*, 1994, **116**, 3449. (*j*) E. B. Brouwer, J. A. Ripmeester and G. D. Enright, *J. Incl. Phenom. Mol. Recognit. Chem.*, 1996, **24**, 1. (*k*) S. Udomsub and S. Hannongbua, *J. Chem. Soc., Faraday Trans.*, 1997, **93**, 3045. (*l*) A. Varnek, S. Helissen, G. Wipff and A. Collet, *J. Comput. Chem.*, 1998, **19**, 820.
9 T. P. Lybrand, J. A. McCammon and G. Wipff, *Proc. Natl. Acad. Sci. USA*, 1986, **83**, 833.
10 (*a*) B. Owenson, R. D. MacElroy and A. Pohorille, *J. Am. Chem. Soc.*, 1988, **110**, 6992. (*b*) B. Owenson, R. D. MacElroy and A. Pohorille, *THEOCHEM*, 1988, **179**, 467.
11 S. Boudon and G. Wipff, *J. Chim. Phys. Phys.–Chim. Biol.*, 1991, **88**, 2443.
12 S. Boudon, A. Decian, J. Fischer, M. W. Hosseini, J.-M. Lehn and G. Wipff, *J. Coord. Chem.*, 1991, **23**, 113.
13 A. Bianchi, S. Mangani, M. Micheloni, V. Nanini, P. Orioli, P. Paoletti and B. Seghi, *Inorg. Chem.*, 1985, **24**, 1182.
14 N. Walker and D. D. Stuart, *Acta Crystallogr., Sect. A*, 1983, **39**, 158.
15 A. Altamore, G. Cascarano, C. Giacovazzo and A. Guagliardi, *J. Appl. Crystallogr.*, 1993, **26**, 343.
16 G. M. Sheldrick, *SHELX-93*, Program for Crystal Structure Refinement, University of Göttingen, 1993.
17 *International Tables for X-Ray Crystallography*, Kynoch Press, Birmingham, England, 1974.
18 A. D. MacKerrel, Jr., J. Wiórkiewicz-Kuczera and M. Karplus, *J. Am. Chem. Soc.*, 1995, **117**, 11946.
19 B. R. Brooks, R. Bruccoleri, B. Olafson, D. States, S. Swaminathan and M. Karplus, *J. Comput. Chem.*, 1983, **4**, 187.
20 J. P. Ryckaert, G. Gicotte and H. J. C. Berendson, *J. Comput. Chem.*, 1977, **23**, 327.
21 C. K. Johnson, *ORTEP, Report ORNL-3794*, Oak Ridge National Laboratory, Oak Ridge, TN, 1971.

Paper 9/06736A